Large-Area 3D Chiral Plasmonic Structures

Bettina Frank,[†] Xinghui Yin,[†] Martin Schäferling,[†] Jun Zhao,[†] Sven M. Hein,[†] Paul V. Braun,[‡] and Harald Giessen[†,*]

[†]4th Physics Institute and Research Center SCoPE, University of Stuttgart, Pfaffenwaldring 57, 70569 Stuttgart, Germany and [‡]Department of Material Science and Engineering, Beckman Institute, University of Illinois at Urbana—Champaign, Urbana, Illinois 61801, United States

ABSTRACT We manufacture large-area plasmonic structures featuring 3-dimensional chirality by colloidal nanohole lithography. By varying the polar rotating speed of the samples during gold evaporation, we can fabricate spiral-type ramp nanostructures. The optical properties show chiroptical resonances in the 100 to 400 THz frequency region (750 to 3000 nm), with circular dichroism values of up to 13%. Our method offers a simple low-cost manufacturing method of cm^2-sized chiral plasmonic templates for chiroptical applications such as stereochemical enantiomer sensors.

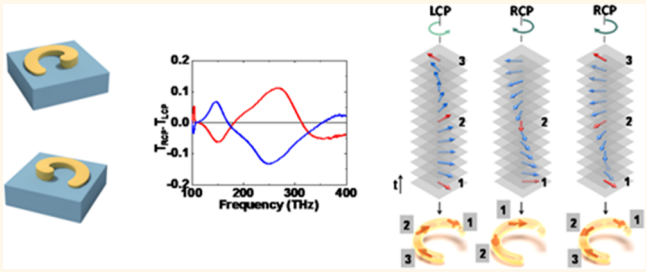

KEYWORDS: hole-mask colloidal nanolithography · large-area chiral gold nanostructures · plasmonics · chirality · circular dichroism · dipole model

Enantiomer sensing is an important tool in analytical chemistry, as many molecules, and in particular biomolecules such as amino acids, proteins, or sugars, are chiral. According to Lord Kelvin, any geometrical figure or group of points is defined as chiral if its mirror image cannot be made to coincide with itself.[1] Chirality in stereochemistry means that a molecule has a left- and a right-handed version, which are called enantiomers. Although enantiomers cannot be superposed onto each other geometrically, they possess the same chemical and physical properties and cannot be distinguished by structural analysis. However, there is one feature where enantiomers are different: their interaction with other chiral entities, in particular circularly polarized light. One resulting effect is called circular dichroism (CD) and describes the absorbance difference between left- and right-handed circularly polarized light for each enantiomer. The chiral interaction of such molecules with electromagnetic radiation is extremely weak, thus the motivation for finding a mechanism to enhance the resulting optical signal is high. One possible enhancement pathway is through chemical binding of chiral molecules onto metal particles. The electronic absorbance of the specific molecule might be enhanced due to the proximity of metal particles, whose surface plasmon frequency is in resonance with the electronic transition of the molecule.[2] Hence, chirality is transferred upon achiral objects by formation of a molecule—metal—particle complex.[3,4] Using CD spectroscopy, these synthetically optical active particles create CD signals at the plasmon resonance frequency of the metal nanoparticle. Theoretical studies of such systems in various arrangements[5,6] have shown that two mechanisms compose the CD effect. First, the electromagnetic field within the molecule is modified due to the metal nanoparticle surface plasmon. Second, the molecule induces chiral currents inside the metal particle.

Theory[7−10] describes the interaction of any chiral material with electromagnetic radiation and also suggests planar and 3D chiral[11] as well as achiral metallic structures[12,13] in the nanometer size range to create chiral electromagnetic fields by themselves. Therefore, such structures are expected to have strong interaction with attached chiral objects in regions of highest field intensity. There are even superchiral solutions of Maxwell's equations,[14] which have higher chiral asymmetry than circularly

* Address correspondence to giessen@physik.uni-stuttgart.de.

Received for review May 10, 2013 and accepted June 27, 2013.

Published online June 27, 2013
10.1021/nn402370x

polarized light. This has already been realized in experiment by either using a reflection geometry setup[15] or by means of planar chiral nanostructures.[16,17] Both arrangements have proven their capability as ultrasensitive enantioselective systems. As already expected, achiral plasmonic structures[18] become chiral by interaction with a chiral molecular layer when using far-field coupling between the layer and plasmonic structure.

The CD enhancement is expected to be even larger if chiral plasmonic nanostructures interact with chiral molecules. There are two approaches to obtain chiral metallic structures. First, metal nanoparticles are arranged in a helical fashion using aggregation and self-assembly effects.[19−22] Their interaction with circularly polarized light results in pronounced CD signals due to electromagnetic coupling between plasmonic particles. Second, fabrication of planar[23−26] chiral plasmonic metal structures, ranging from macroscopic sizes down to nanometer dimensions is possible using lithographic techniques. Even 3D geometries are feasible, for example, stacked and twisted rosette structures[27,28] with a chiroptical response in the GHz regime. Electron-beam lithography opens the door for uncountable fabrication possibilities as, for example, stacked gammadions[29] and twisted crosses[30] or twisted layers of nanorods.[31] Another prominent example is stereometamaterials,[32] where the chiral optical response of pairs of stacked splitring resonator structures depends on their twist angle.[33,34] Chiral plasmonic oligomers, fabricated in various handed arrangements,[35−37] create a multitude of modes with a chiral optical response. Finally, direct laser writing provides an attractive and flexible but challenging fabrication approach for 3D chiral[38] and bichiral[39] structures, which can be used as circular polarizing devices in the mid-infrared wavelength range. The combination of direct laser writing and electron-beam lithography[40] is even more advanced and enables fabrication of complex 3D metal structures with optical response in the visible and near-infrared spectral region.

However, this diversity of chiral metallic structures either exhibits a chiroptical response in the far-infrared, or metal structures are arranged only over a few square micrometers, which makes CD measurements using commercial CD spectrometer setups very difficult. Self-assembled chiral structures are fabricated by complex techniques such as DNA-origami or DNA scaffolds. For potential enantiomer sensing substrates, it is highly desirable to fabricate 3D chiral gold structures in the nanometer size range, distributed over macroscopic areas, using a fast and easy to perform fabrication technique that works in the low-cost price regime. Here, we demonstrate a novel method to fabricate left- and right-handed 3D chiral gold nanostructures on square centimeter sized glass substrates by colloidal hole-mask lithography in combination with tilted-angle rotation evaporation. Furthermore, we discuss the chiral optical response of our fabricated structures in detail with the help of FTIR measurements and develop a dipole model to explain the differences in transmittance between left-handed and right-handed circularly polarized light.

RESULTS AND DISCUSSION

We use a combination of hole-mask lithography and subsequent tilted angle evaporation to fabricate chiral gold nanostructures over square centimeters. Hole-mask lithography has already been introduced by the work of Fredriksson[41] and refined by our group.[42,43] It is a quite flexible and easy method for the fabrication of metallic nanostructures. For structure evaporation, we use our tilted-angle rotation setup,[44−47] which is a modified thermal evaporation machine with flexible sample holder where the hole-mask substrate is mounted. This sample holder can be rotated in θ and φ direction, as indicated in Figure 1a, utilizing a stepper motor construction. Our homemade stepper motor control software enables precise regulation of the sample movement and position, which is why the evaporation of very complex structures is possible. Here, we describe the deposition of left- and right-handed 270° 3D chiral gold structures as sketched in Figure 1a. The rotation direction of the sample holder is responsible for the handedness of the structure. It is defined by the sign of rotation velocity, that is, by the sign of periodic change of the polar angle φ. We define the negative sign of the rotation velocity as left-handed rotation and therefore left-handed structures are produced. Throughout this article, we indicate the handedness of our structures by colors, where blue means left-handed and red represents right-handed structures. Owing to our geometrical model,[42] we chose a fixed azimuthal angle θ of 22.5°. To obtain spiral-like chiral structures, the structure height has to be inhomogeneous. Therefore, we have to accelerate the rotation speed during metal deposition. In the beginning, the sample holder is rotating quite slowly so that a large amount of material passes through the hole and is deposited on the glass substrate. Subsequently, we slowly increase the rotation velocity, which causes less material to reach the glass substrate and the structure height becomes thinner. With proceeding evaporation, more material is deposited around the hole in the hole-mask, and, therefore, its diameter shrinks. This affects the evaporated structure width. In Figure 1b, we describe the sample movement graphically for the evaporation of chiral structures. A final clear-tape lift-off process removes the PMMA mask from the glass substrate. Subsequent immersion into NEP solution for several minutes and oxygen plasma cleaning remove remaining PMMA.

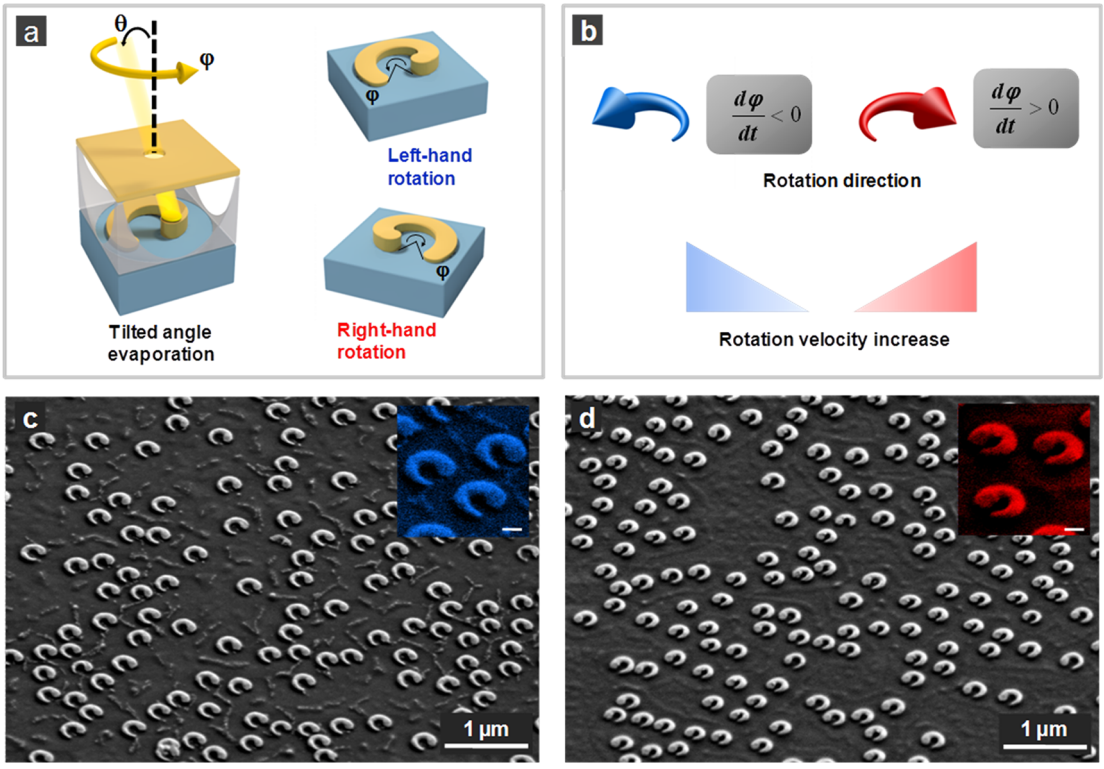

Figure 1. (a) Hole-mask lithography and tilted angle rotation evaporation create 270° left- and right-handed 3D chiral structures over a large area of 1 cm^2. Blue indicates left-handed rotation, red represents right-handed rotation. (b) Rotation parameters during evaporation. The variation of angle φ in the negative direction represents left-handed rotation while the variation in positive direction leads to right-handed rotation of the sample. To obtain inhomogeneous structures, rotation velocity has to be accelerated. (c) SEM micrograph of left-handed structures. The inset shows a high magnification cutout. (d) Image of a right-handed enantiomer sample with high magnification inset. The inset scale bar is 100 nm.

SEM studies illustrate the created chiral gold structures, arbitrarily arranged according to the initial polystyrene (PS) sphere pattern over a large area of one square centimeter. Figure 1 panels c and d show typical overview images. The insets illustrate corresponding high magnification cut-outs. To determine structure dimensions we estimate the outer diameter and the structure width from averaged measurements over several representative areas taken from different spots on the sample. Our outer structure diameters average to 260 nm and the structure widths shrink from about 90 nm down to roughly 20 nm.

To determine the height profile, we perform AFM measurements. Figure 2 shows a 3D plot of our structures extracted from AFM raw data, depicted in the inset. This confirms the inhomogeneous structure dimensions, which render our structures 3D chiral.

In the following, we discuss particularly the optical spectra of left-handed structures. The results of right-handed structures are shown as well. With respect to their chiral properties, the related physics is exactly mirror symmetric. Experimental spectra are depicted in the left column of Figure 3. The right column shows the results of a simple numerical model.

First, we show spectra measured with linearly polarized light in the *x* and *y* direction, plotted in black and gray, respectively. The polarization directions are illustrated in the insets of Figure 3a. The transmittance spectra are similar for left- and right-handed structures. To understand the mode pattern, it is helpful to compare our data with the plasmonic resonances of planar split-ring resonator structures.[46] For *x*-polarized light, two resonances are excited, one at 150 THz the other one at roughly 320 THz. In *y* polarization, there is mainly

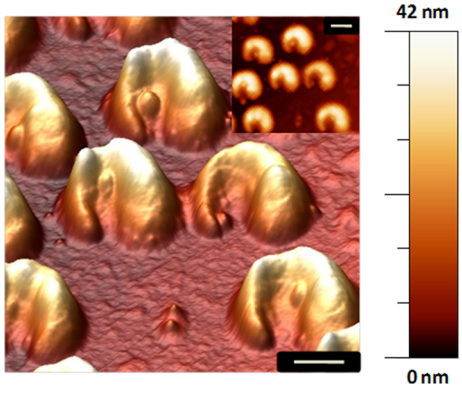

Figure 2. Overview AFM image containing a 3D plot and AFM raw data. The irregular structure width and the inhomogeneous structure height make clear that our structures are 3D chiral. The scale bars in the image and in the inset are 200 nm.

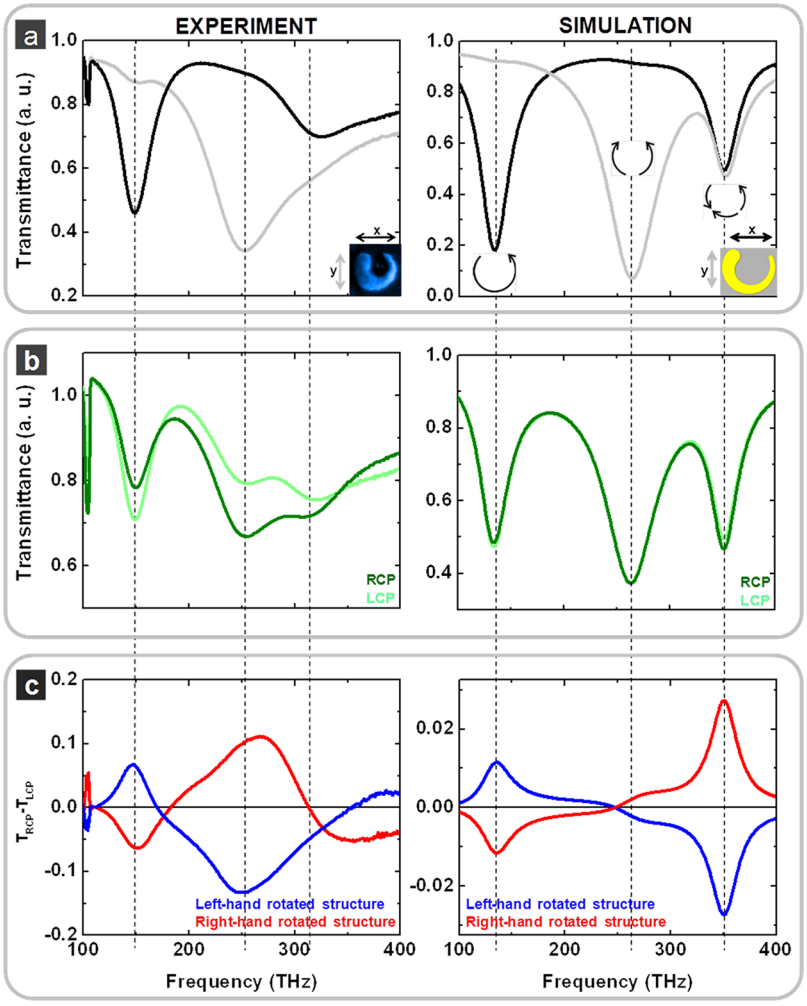

Figure 3. (a) Transmittance spectra for linearly polarized light. For the black curve, the electric field vector is polarized in the *x* direction, which excites the fundamental and the third order resonance. For polarization in the *y* direction, the gray curve exhibits the second order resonance. (b) Circularly polarized light excites all the three resonances. (c) Transmittance differences between left- and right-handed circularly polarized light $\Delta T = T_{RCP} - T_{LCP}$ for left- and right-handed structures are shown. There are distinct peaks at the three resonance positions. The second- and third-order-resonance merge to one broader peak for the transmission difference signal. 300 THz corresponds to 1 μm wavelength.

one resonance dip in the transmittance spectrum located at 250 THz. The arrow diagrams in the simulated spectrum (indicating the current distribution for the different modes) of Figure 3a clarify the character of the resonances. For *x*-polarized light, the first- and third-order resonances are excited while the second-order resonance mode is excited for the electric field vector polarized in *y* direction. Owing to structure asymmetry, the third order resonance is weakly excited in experiment and in simulation using *x*- as well as *y*-polarized light.

To determine the chiral properties of our structures, we study transmittance using circularly polarized light. For these measurements, we insert an infrared quarter wave plate into the light path between polarizer and sample. Here, we define left-handed circularly polarized (LCP) light as the light whose electric field vector is performing a left-handed screw during propagation towards the sample. In Figure 3b the light green curve describes the transmission spectrum of our left-handed structure for left-handed circularly polarized light and the dark green curve for right-handed circularly polarized light. Here we measure in forward configuration, which means that the light which excites the plasmon resonance impinges from the top onto the structures. Apparently, there are differences between the spectra measured with LCP light and RCP light, confirming the chiral characteristics of our structures. All three resonance modes are excited and situated at the same frequency positions for both LCP and RCP, which are the same as for linearly polarized incident light. The dashed lines in Figure 3 help to compare the resonance positions of all the measured spectra. The resonance at 150 THz is the fundamental mode, and the ones at 250 THz and 320 THz are attributed to the second and third order resonance, respectively. At the fundamental resonance, transmittance for LCP light is smaller than for RCP light, while for

the second- and third-order resonances this behavior is reversed.

Our main interest lies in the chiral optical properties of our structures, which are described by circular dichroism (CD). Circular dichroism is defined as the difference in absorbance for right- and left-handed circularly polarized light. As in ref 30, our FTIR setup only allows reflectance measurement for circularly polarized light in a very small frequency range. Within this spectral region the differences between absorbance and (1 − transmittance) are compared, indicating no significant deviations. Therefore, we calculate the transmittance difference (ΔT) between RCP and LCP light in order to determine the chiral properties of our sample. This is shown in Figure 3c. Owing to our fabrication method, all structures are oriented in the same direction, exhibiting no rotational symmetry of the arrangement. Thus, we expect contributions of polarization conversion to our measured $\Delta T_{\text{RCP-LCP}}$ spectra due to elliptic birefringence arising from the biaxiality of our sample. An overall structure arrangement in C_3- or C_4-symmetry would make the sample uniaxial[35] and suitable for CD measurements that are not hampered by polarization conversion. So far we are not able to fabricate structures in a C_4-symmetric arrangement. However, to obtain the chiral response, we use the calculation introduced in refs 35 and 48, assuming that the mean value between top and bottom illumination of the transmittance difference between RCP light and LCP light determines correct chiral ΔT values. According to this we have to calculate our $\Delta T_{\text{RCP-LCP}}$ spectra using $\Delta T = 0.5(\Delta T_{(\text{RCP-LCP})\text{top}} - \Delta T_{(\text{RCP-LCP})\text{bottom}})$. Therefore, we measure transmittance of our left- and right-handed samples from both illumination directions on the same sample spot in each case. We find qualitative agreement between maximum CD response and position for the fundamental resonance. At this resonance, the ΔT spectrum exhibits positive values. This changes at roughly 170 THz, so the second- and third-order resonances possess a negative sign. The two resonances merge into one broad ΔT resonance, displaying a maximum at 250 THz. We also compare ΔT spectra between left-handed and right-handed chiral structures. The spectrum of right-handed rotated structures is plotted in red in Figure 3c and shows good mirror symmetry when compared with the spectrum of the left-handed structures, which is expected for enantiomers.

We also simulate transmittance spectra for LCP light and RCP light. The right-hand side of Figure 3 shows our model, a circular ramp with increasing width, which describes the excited mode structure qualitatively and has the same important features as the experiment. The model was optimized to fit the relative positions of the resonances as well as the signs of the respective circular dichroism signals. A more detailed representation of the actual structure geometry and modeling of the nonperiodic structure distribution would be necessary to achieve a quantitative description. However, the obtained qualitative agreement is sufficient to gain further insight into the chiral properties of our nanostructures.

To describe the origin of the observed resonance modes, we calculate from our simulations the current oscillations and the electric field distributions for each resonance position, as depicted in Figure 4. Here we only show the modes for excitation with linearly polarized light. Resonances excited by circularly polarized light can be decomposed taking into account $\sigma_{\pm} = x \pm iy$. Because of the asymmetric structure shape the excited current oscillations and therefore the electric field distributions are asymmetric as well. We show in Figure 4a a cross-section through our modeled structure, displaying a snapshot of the current distributions at each resonance position. In Figure 4b we depict the corresponding *z*-component of the electric field distribution that arises from the current distribution in 4a. In column (i), the current flow of the first order resonance at 150 THz is excited by light that is linearly polarized in *x*-direction and, thus, parallel to the structure gap. Such light excites an electron oscillation within our gold structure that represents the fundamental particle plasmon mode. Figure 4b depicts in image i the electric field that arises due to charge separation in the structure. According to the incident polarization, this electric field is oriented in the *x*-direction parallel to the structure gap and forms an oscillating dipole. Column (ii) describes the current oscillation and the electric field distribution for the second order resonance at 250 THz. This resonance is excited by *y*-polarized light perpendicular to the structure gap. The current oscillation exhibits one node. Hence, a dipolar electric field is oriented in *y*-direction. In column (iii) the current oscillation and the electric field distribution of the third order resonance at 320 THz are described. The current oscillation of the third order mode has two nodes, corresponding to an electric field with quadrupolar character.

In the following, we are going to explain the origin of the chiroptical response of our structures. In Figure 5 we depict the excitation scheme of the above-described current oscillations excited by circularly polarized light. The leftmost column illustrates the fundamental mode, the center one the second order mode, and the right column depicts the third order mode.

We use circularly polarized light that propagates toward the structure. In our illustration, we describe the electric field vector by a rotating arrow at several points in time. Circularly polarized light impinges on the structure and excites the plasmon oscillation, which is denoted as red arrows inside the structure and therefore represents electric dipoles. We discuss

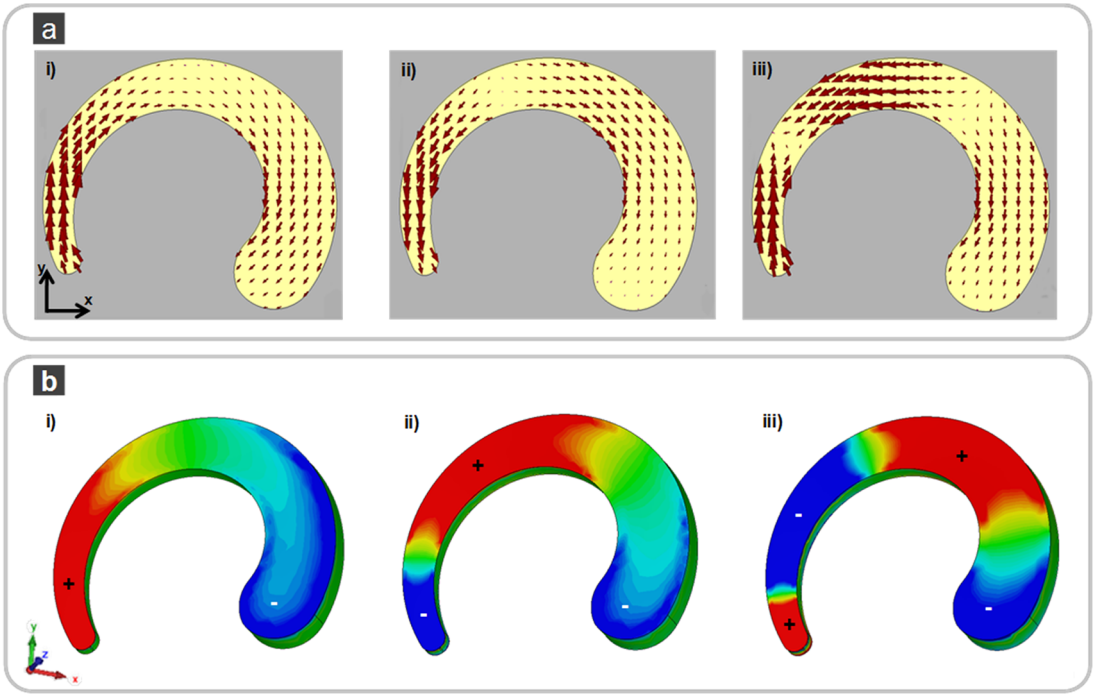

Figure 4. Resulting (a) current and (b) *z*-component of the electric field distributions of the electron oscillations. (i) First-order resonance without any node, which results in a dipolar electric field parallel to the structure opening (polarization in *x*-direction). The second-order resonance with one node in the current oscillation is described in panel ii. The resulting electric field distribution results in a dipole field perpendicular to the structure gap (polarization in y-direction). In panel iii the current-oscillation and the electric field distribution of the third order-resonance are shown, which is also excited for *x*-polarized light.

this for all resonance positions of our left-handed structures and start with the excitation scheme of the first-order resonance, which is plotted at the left side of Figure 5. Here, LCP-light experiences maximum absorbance, which means that the screw of the circularly polarized light fits the structure's twist. Hence, the light excites the fundamental mode and is absorbed. First, the red arrow marked with number 1 in the light wave starts the electron oscillation at the highest point of the structure. Further propagation of LCP light along the structure surface up to point 2 leads to progressive excitation of the electron oscillation, and we place another electric dipole parallel to the structure gap. Finally, at point 3 one more electric dipole forms in the structure, which is excited by the electric field vector oscillating in direction 3. In our picture, there are now three electric dipoles aligned in series. For the second- and third-order resonance the opposite polarization, namely RCP light, is more strongly absorbed. In the center column of Figure 5, the second-order mode is illustrated. The red electric-field vectors marked with 1 and 2 excite electric dipoles 1 and 2 in the structure, while RCP light circulates along the structure. The dipole arrangement indicates that the second order resonance mode can only be excited due to the round and inhomogeneous shape of our structures. The two dipoles are aligned oppositely. Finally, within the third-order resonance on the right side in Figure 5, there are again three electric dipoles excited, marked by number 1−3. In this case the electric dipoles are facing each other and therefore the oscillation exhibits two nodes. The difference to the fundamental mode is only the orientation of the second dipole. This explains why the third-order mode is excited by light with opposite handedness compared to the fundamental mode.

From this, the origin of the circularly polarized transmittance difference in the optical spectra of our 3D chiral structures becomes clear: Excitation of the first order resonance in the left-handed chiral structure with RCP-light leads to less absorbance, because this type of polarized light counter-circulates with respect to the structure's twist. Equivalent reasoning for the second and third order resonances yields a low excitation efficiency for LCP-light, whose handedness does not match with the arrangement of the plasmonic dipoles of the higher order modes in the twisted structure.

On the basis of this dipole model, we utilize a plasmon hybridization model[49] to clarify the resonance position, which is illustrated at the bottom of Figure 5. The first order resonance possesses the lowest energy configuration because the three dipoles are oriented in series and therefore attract each other. Applying the second order resonance to the hybridization picture, we have to consider opposite dipole alignment. Because of this configuration, the two dipoles repel each other and are therefore settled at a higher energy level. The third order resonance with

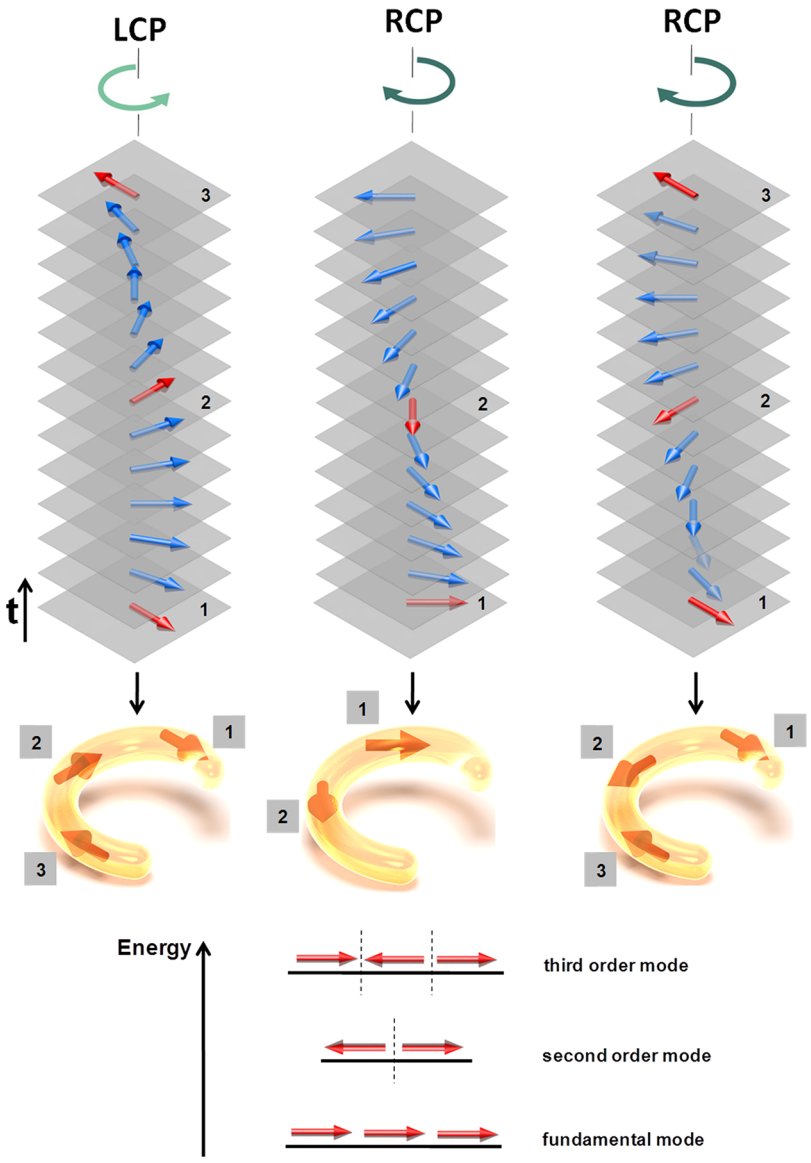

Figure 5. Formation and character of ΔT peaks in the left-handed chiral plasmonic structure. Circularly polarized light that propagates toward the structure is illustrated by a rotating arrow scheme that represents a dipolar incident electric field vector. This motivates the application of an approximate dipole picture to describe the resonance spectra. The red colored and numbered arrows in the light wave are responsible for plasmon excitation in the fabricated structures. These electron oscillations are also described by arrows in the structure, which result in an electric dipole. Corresponding to the numbers in the structure and in the illustrated light wave, the overall plasmon resonance is excited. This is shown for all the three resonance modes and summarized in a plasmonic hybridization model.

its two nodes occupies the highest energy level, as the three electric dipoles are antiparallel and therefore repel each other. This scheme explains the connection between mode structure and circular symmetry in chiral plasmonic structures. Finally, the metal structures with right-handed structural symmetry behave exactly opposite.

In the Supporting Information, we additionally study theoretically the dependence of chiral transmittance on the structure length as well as the consequences on the mode symmetry. In this case, the CD sign of the second order mode can flip due to the modified plasmon hybridization.

CONCLUSION

We have demonstrated that colloidal hole-mask lithography in combination with tilted angle rotation evaporation is a quite flexible fabrication method for left- and right-handed 3D chiral plasmonic structures, covering square centimeters of glass substrates. To determine their chiral optical response, we have performed FTIR measurements with circularly polarized light and found significant transmittance differences between RCP light and LCP light (ΔT). We found ΔT maxima and minima at the plasmonic resonance positions, which are mirrored for the two enantiomers. Furthermore, we have developed a dipole model to explain the interaction between circularly polarized light

and our plasmonic structures. This has clarified the origin of the positive and negative signs of transmittance mode differences between RCP light and LCP light and their relation with the chirality of the structure.

Our work could find applications as substrates for plasmonically enhanced detection of different enantiomers in biomolecular substances with commercial CD spectrometers.

METHODS

Structure Fabrication. First we outline the most important steps of this fabrication technique. We spin-coat a PMMA layer of approximately 200 nm thickness onto a functionalized glass substrate, which is subsequently covered with a submonolayer of polystyrene (PS) nanospheres of about 100 nm diameter. On top of this system, a gold film of 20 nm is evaporated using an Edwards E 306 thermal evaporator to protect the PMMA from further treatment. After this, the arbitrarily spread PS particles are removed by a soft ultrasonic bath in water. This yields a gold layer on top of the PMMA substrate including holes of roughly 100 nm diameter. A final isotropic oxygen plasma etching step removes the PMMA through these holes and to some extent underneath the gold layer until the glass substrate is reached. This creates adequate cavities to make space for the evaporation process. The functional principle of our hole masks is the following: in high vacuum, gold is evaporated, impacts on the mask and passes through the holes. These holes form a gold vapor beam that operates as pencil that writes the sample. A certain tilt angle of the sample in azimuthal direction θ and sample rotation in polar direction φ opens the door to the fabrication of a large variety of metal structures in the nanometer size range according to the diameter of the used PS spheres. This is schematically illustrated in Figure 1a. Due to polydisperity of the PS spheres, the mask is expected to have slightly different hole sizes, and eventually produces slightly inhomogeneous gold structures. AFM measurements are carried out using a Veeco Dimension Icon in combination with NanoAndMore TAP300-AR-G-50 tips for tapping mode in air. AFM analysis is done by the software WSxM.[50]

Optical Measurements. To determine the chiral optical response of our structures, we perform optical measurements using a Fourier-transform infrared spectrometer (FTIR) Bruker Vertex 80 combined with a Bruker Hyperion II infrared microscope. For our measurements, we use an MCT-detector and a Si-diode according to the corresponding frequency range. Optical spectra are obtained by normal light incidence in transmission mode. The incident polarization is set with an infrared polarizer and a broadband infrared quarter wave plate (700 nm−2500 nm, B. Halle Nachfl., Berlin). All measured spectra are normalized with respect to a bare glass substrate.

Simulations. To verify our measurements, we simulate the structure geometry using the frequency domain solver of CST Microwave studio. Owing to an inhomogeneous size distribution of our structures, we have to modify the size parameters of our model slightly in order to match the resonance frequency positions. Furthermore, we choose the refractive index of glass $n = 1.5$ and describe the permittivity of bulk gold by a Drude model with plasma frequency $\omega_p = 1.37 \times 10^{16}$ Hz and damping constant $\kappa = 1.2 \times 10^{14}$ Hz.

Conflict of Interest: The authors declare no competing financial interest.

Acknowledgment. We acknowledge M. Hentschel for his help and discussions about the circular dichroism measurements. We acknowledge the Alexander von Humboldt foundation (Bessel Prize) and the BW Stiftung "Spitzenforschung" for P.V.B. The authors acknowledge support through the Advanced Grant COMPLEXPLAS from the European Research Council (ERC). This work was financially supported by BMBF (3D Metamat) and DFG (FOR 730, SPP1391).

Supporting Information Available: Relation between plasmonic structure length and handedness of the CD response. This material is available free of charge *via* the Internet at http://pubs.acs.org.

REFERENCES AND NOTES

1. Thomson, W. H.; Kelvin, L. *Baltimore Lectures*; C. J. Clay and Sons: London, 1884; Vol. 1904, pp 436619.
2. Lieberman, I.; Shemer, G.; Fried, T.; Kosower, E. M.; Markovich, G. Plasmon-Resonance-Enhanced Absorption and Circular Dichroism. *Angew. Chem., Int. Ed.* **2008**, *47*, 4855–4857.
3. Slocik, J. M.; Govorov, A. O.; Naik, R. R. Plasmonic Circular Dichroism of Peptide-Functionalized Gold Nanoparticles. *Nano Lett.* **2011**, *11*, 701–705.
4. Maoz, B. M.; Chaikin, Y.; Tesler, A. B.; Bar Elli, O.; Fan, Z.; Govorov, A. O.; Markovich, G. Amplification of Chiroptical Activity of Chiral Biomolecules by Surface Plasmons. *Nano Lett.* **2013**, *13*, 1203–1209.
5. Govorov, A. O.; Fan, Z.; Hernandez, P.; Slocik, J. M.; Naik, R. R. Theory of Circular Dichroism of Nanomaterials Composing Chiral Molecules and Nanocrystals: Plasmon Enhancement, Dipole Interactions, and Dielectric Effects. *Nano Lett.* **2010**, *10*, 1374–1382.
6. Govorov, A. O. Plasmon-Induced Circular Dichroism of a Chiral Molecule in the Vicinity of Metal Nanocrystals. Application to Various Geometries. *J. Phys. Chem. C* **2011**, *115*, 7914–7923.
7. Fan, Z.; Govorov, A. O. Plasmonic Circular Dichroism of Chiral Metal Nanoparticle Assemblies. *Nano Lett.* **2010**, *10*, 2580–2587.
8. Fan, Z.; Govorov, A. O. Helical Metal Nanoparticle Assemblies with Defects: Plasmonic Chirality and Circular Dichroism. *J. Phys. Chem. C* **2011**, *115*, 13254–13261.
9. Engheta, N.; Jaggard, D. L. Electromagnetig Chirality and Its Applications. *IEEE Antennas Propagat. Soc. Newslett.* **1988**, *30*, 6–12.
10. Engheta, N.; Kowarz, M. W. Antenna Radiation in the Presence of a Chiral Sphere. *J. Appl. Phys.* **1990**, *67*, 639–647.
11. Schäferling, M.; Dregely, D.; Hentschel, M.; Giessen, H. Tailoring Enhanced Optical Chirality: Design Principles for Chiral Plasmonic Nanostructures. *Phys. Rev. X* **2012**, *2*, 031010.
12. Schäferling, M.; Yin, X.; Giessen, H. Formation of Chiral Fields in a Symmetric Environment. *Opt. Express* **2012**, *20*, 26326–26336.
13. Davis, T. J.; Hendry, E. Superchiral Electromagnetic Fields Created by Surface Plasmons in Nonchiral Metallic Nanostructures. *Phys. Rev. B* **2013**, *87*, 085405.
14. Tang, Y.; Cohen, A. E. Optical Chirality and Its Interaction with Matter. *Phys. Rev. Lett.* **2010**, *104*, 163901.
15. Tang, Y.; Cohen, A. E. Enhanced Enantioselectivity in Excitation of Chiral Molecules by Superchiral Light. *Science* **2011**, *332*, 333–336.
16. Hendry, E.; Carpy, T.; Johnston, J.; Popland, M.; Mikhaylovskiy, R. V.; Lapthorn, A. J.; Kelly, S. M.; Barron, L. D.; Gadegaard, N.; Kadodwala, M. Ultrasensitive Detection and Characterization of Biomolecules Using Superchiral Fields. *Nat. Nanotechnol* **2010**, *5*, 783–787.
17. Quidant, R.; Kreuzer, M. Plasmons Offer a Helping Hand. *Nat. Nanotechnol.* **2010**, *5*, 762–763.
18. Abdulrahman, N. A.; Fan, Z.; Tonooka, T.; Kelly, S. M.; Gadegaard, N.; Hendry, E.; Govorov, A. O.; Kadodwala, M. Induced Chirality through Electromagnetic Coupling between Chiral Molecular Layers and Plasmonic Nanostructures. *Nano Lett.* **2012**, *12*, 977–983.
19. Mastroianni, A. J.; Claridge, S. A.; Alivisatos, A. P. Pyramidal and Chiral Groupings of Gold Nanocrystals Assembled Using DNA Scaffolds. *J. Am. Chem. Soc.* **2009**, *131*, 8455–8459.
20. Shen, X.; Song, C.; Wang, J.; Shi, D.; Wang, Z.; Liu, N.; Ding, B. Rolling Up Gold Nanoparticle-Dressed DNA Origami into Three-Dimensional Plasmonic Chiral Nanstructures. *J. Am. Chem. Soc.* **2012**, *134*, 146–149.

21. (a) Kuzyk, A.; Schreiber, R.; Fan, Z.; Pardatscher, G.; Roller, E.-M.; Högele, A.; Simmel, F. C.; Govorov, A. O.; Liedl, T. DNA-Based Self-Assembly of Chiral Plasmonic Nanostructures with Tailored Optical Response. *Nature* **2012**, *483*, 311–314. (b) Shen, X. B.; Asenjo-Garcia, A.; Liu, Q.; Jiang, Q.; García de Abajo, J.; Liu, N.; Ding, B. Q. Three-Dimensional Plasmonic Chiral Tetramers Assembled by DNA Origami. *Nano Lett.* **2013**, *13*, 2128.
22. Gérard, V. A.; Gun'ko, Y. K.; Defrancq, E.; Govorov, A. O. Plasmon-Induced CD Response of Oligonucleotide-Conjugated Metal Nanoparticles. *Chem. Commun.* **2011**, *47*, 7383–7385.
23. Papakostas, A.; Potts, A.; Bagnall, D.; Prosvirnin, S.; Coles, H.; Zheludev, N. Optical Manifestations of Planar Chirality. *Phys. Rev. Lett.* **2003**, *90*, 107404.
24. Schwanecke, A. S.; Krasavin, A.; Bagnall, D. M.; Potts, A.; Zayats, A. V.; Zheludev, N. Broken Time Reversal of Light Interaction with Planar Chiral Nanostructures. *Phys. Rev. Lett.* **2003**, *91*, 247404.
25. Kuwata-Gonokami, M.; Saito, N.; Ino, Y.; Kauranen, M.; Jefimovs, K.; Vallius, T.; Turunen, J.; Svirko, Y. Giant Optical Activity in Quasi-Two Dimensional Planar Nanostructures. *Phys. Rev. Lett.* **2005**, *95*, 227401.
26. Valev, V. K.; Smisdom, N.; Silhanek, A. V.; De Clercq, B.; Gillijns, W.; Ameloot, M.; Moshchalkov, V. V; Verbiest, T. Plasmonic Ratchet Wheels: Switching Circular Dichroism by Arranging Chiral Nanostructures. *Nano Lett.* **2009**, *9*, 3945–3948.
27. Rogacheva, A. V.; Fedotov, V. A.; Schwanecke, A. S.; Zheludev, N. I. Giant Gyrotropy Due to Electromagnetic Coupling. *Phys. Rev. Lett.* **2006**, *97*, 177401.
28. Plum, E.; Zhou, J.; Dong, J.; Fedotov, V.; Koschny, T.; Soukoulis, C.; Zheludev, N. Metamaterial with Negative Index due to Chirality. *Phys. Rev. B* **2009**, *79*, 035407.
29. Decker, M.; Klein, M. W.; Wegener, M.; Linden, S. Circular Dichroism of Planar Chiral Magnetic Metamaterials. *Opt. Lett.* **2007**, *32*, 856–858.
30. Decker, M.; Ruther, M.; Kriegler, C. E.; Zhou, J.; Soukoulis, C. M.; Linden, S.; Wegener, M. Strong Optical Activity from Twisted-Cross Photonic Metamaterials. *Opt. Lett.* **2009**, *34*, 2501–2503.
31. Zhao, Y.; Belkin, M. A.; Alù, A. Twisted Optical Metamaterials for Planarized, Ultrathin Broadband Circular Polarizers. *Nat. Commun.* **2012**, *3*, 870.
32. Liu, N.; Liu, H.; Zhu, S.; Giessen, H. Stereometamaterials. *Nat. Photon.* **2009**, *3*, 157–162.
33. Liu, H.; Cao, J. X.; Zhu, S. N.; Liu, N.; Ameling, R.; Giessen, H. Lagrange Model for the Chiral Optical Properties of Stereometamaterials. *Phys. Rev. B* **2010**, *81*, 241403(R).
34. Liu, N.; Giessen, H. Coupling effects in optical metamaterials. *Angew. Chemie, Int. Ed.* **2010**, *49*, 9838.
35. Hentschel, M.; Schäferling, M.; Weiss, T.; Liu, N.; Giessen, H. Three-Dimensional Chiral Plasmonic Oligomers. *Nano Lett.* **2012**, *12*, 2542–2547.
36. Hentschel, M.; Wu, L.; Schäferling, M.; Bai, P.; Li, E. P.; Giessen, H. Optical Properties of Chiral Three-dimensional Plasmonic Oligomers at the Onset of Charge-Transfer Plasmons. *ACS Nano* **2012**, *6*, 10355–10365.
37. Hentschel, M.; Schäferling, M.; Metzger, B.; Giessen, H. Plasmonic Diastereomers: Adding up Chiral Centers. *Nano Lett.* **2013**, *13*, 600–606.
38. Gansel, J. K.; Thiel, M.; Rill, M. S.; Decker, M.; Bade, K.; Saile, V.; von Freymann, G.; Linden, S.; Wegener, M. Gold Helix Photonic Metamaterial as Broadband Circular Polarizer. *Science* **2009**, *325*, 1513.
39. Radke, A.; Gissibl, T.; Klotzbücher, T.; Braun, P. V; Giessen, H. Three-Dimensional Bichiral Plasmonic Crystals Fabricated by Direct Laser Writing and Electroless Silver Plating. *Adv. Mater.* **2011**, *23*, 3018–3021.
40. Staude, I.; Decker, M.; Ventura, M. J.; Jagadish, C.; Neshev, D. N.; Gu, M.; Kivshar, Y. S. Hybrid High-Resolution Three-Dimensional Nanofabrication for Metamaterials and Nanoplasmonics. *Adv. Mater.* **2012**, *25*, 1260–1264.
41. Fredriksson, H.; Alaverdyan, Y.; Dmitriev, A.; Langhammer, C.; Sutherland, D. S.; Zäch, M.; Kasemo, B. Hole-Mask Colloidal Lithography. *Adv. Mater.* **2007**, *19*, 4297–4302.
42. Cataldo, S.; Zhao, J.; Neubrech, F.; Frank, B.; Zhang, C.; Braun, P. V; Giessen, H. Hole-Mask Colloidal Nanolithography for Large-Area Low-Cost Metamaterials and Antenna-Assisted Surface-Enhanced Infrared Absorption Substrates. *ACS Nano* **2012**, *6*, 979–985.
43. Zhao, J.; Zhang, C.; Braun, P. V; Giessen, H. Large-Area Low-Cost Plasmonic Nanostructures in the NIR for Fano Resonant Sensing. *Adv. Mater.* **2012**, *24*, OP247.
44. Kosiorek, A.; Kandulski, W.; Chudzinski, P.; Kempa, K.; Giersig, M. Shadow Nanosphere Lithography: Simulation and Experiment. *Nano Lett.* **2004**, *4*, 1359–1363.
45. Kosiorek, A.; Kandulski, W.; Glaczynska, H.; Giersig, M. Fabrication of Nanoscale Rings, Dots, and Rods by Combining Shadow Nanosphere Lithography and Annealed Polystyrene Nanosphere Masks. *Small* **2005**, *1*, 439–444.
46. Gwinner, M. C.; Koroknay, E.; Fu, L.; Patoka, P.; Kandulski, W.; Giersig, M.; Giessen, H. Periodic Large-Area Metallic Split-Ring Resonator Metamaterial Fabrication Based on Shadow Nanosphere Lithography. *Small* **2009**, *5*, 400–406.
47. Zhao, J.; Frank, B.; Burger, S.; Giessen, H. Large-Area High-Quality Plasmonic Oligomers Fabricated by Angle-Controlled Colloidal Nanolithography. *ACS Nano* **2011**, *5*, 9009–9016.
48. Kuroda, R.; Harada, T.; Shindo, Y. A Solid-State Dedicated Circular Dichroism Spectrophotometer: Development and Application. *Rev. Sci. Instrum.* **2001**, *72*, 3802–3810.
49. Prodan, E.; Radloff, C.; Halas, N. J.; Nordlander, P. A Hybridization Model for the Plasmon Response of Complex Nanostructures. *Science* **2003**, *302*, 419–422.
50. Horcas, I.; Fernández, J. M.; Gómez-Rodriguez, J.; Colchero, J.; Gómez-Herrero, J.; Baro, A. M. WSXM: A Software for Scanning Probe Microscopy and a Tool for Nanotechnology. *Rev. Sci. Instrum.* **2007**, *78*, 013705.